



INSTITUT DE FRANCE
Académie des sciences

Comptes Rendus

Mécanique


Mahdi Chavoshian, Mostafa Taghizadeh and Nima Zamani
Meymian

**Implementation and experimental tests of an impedance control of
pneumatic artificial muscles for isokinetic rehabilitation**

Volume 348, issue 3 (2020), p. 211-233.

<<https://doi.org/10.5802/crmeca.16>>

© Académie des sciences, Paris and the authors, 2020.
Some rights reserved.

 This article is licensed under the
CREATIVE COMMONS ATTRIBUTION 4.0 INTERNATIONAL LICENSE.
<http://creativecommons.org/licenses/by/4.0/>



*Les Comptes Rendus. Mécanique sont membres du
Centre Mersenne pour l'édition scientifique ouverte*
www.centre-mersenne.org



Implementation and experimental tests of an impedance control of pneumatic artificial muscles for isokinetic rehabilitation

Mahdi Chavoshian^a, Mostafa Taghizadeh^{®*,a} and Nima Zamani Meymian^b

^a Faculty of Mechanical and Energy Engineering, Shahid Beheshti University, Tehran, Iran

^b Dept. of Mechanical and Aerospace Engineering, West Virginia University, Morgantown, WV, USA.

E-mails: m_chavoshian@sbu.ac.ir (M. Chavoshian), mo_taghizadeh@sbu.ac.ir (M. Taghizadeh), Nima_Zamani@wvuj.ac (N. Z. Meymian).

Abstract. The impedance control of an pneumatic artificial muscle for isokinetic rehabilitation applications was investigated. Due to the direct contact of rehabilitation robots with the human body, the safety and reliability of these robots are of significant importance. For such applications, position and force must be introduced simultaneously. In this regard, there are two scenarios in which the controller should compromise between the position commands and the resultant force or vice versa. To achieve these goals and considering the safety requirements, a novel control algorithm was proposed, which was identified as a reliable strategy that can be utilized for rehabilitation purposes. The fuzzy sliding mode controller was implemented to control the actuator's velocity (time-varying position signal) to eliminate/reduce chattering and improve the settling time. The performance of the controller using the position-based impedance algorithm was investigated through lab experiments. For experiments, a mechanism consisting of a pneumatic muscle and a pneumatic proportional valve was used, and the control of vertical reciprocating motion of a mass attached to the end of the muscle was investigated. Three different reference signals were used in tests, and the maximum tracking error was measured to be less than 6%. Using the measured error criteria, a parametric study was performed to identify the effects of three impedance parameters on the outputs. The results of the parametric study were reported through response surfaces and sensitivity charts. The presented methods have not been implemented in prior research for controlling a pneumatic muscle, and the results of the experiments were satisfactory.

Keywords. Pneumatic artificial muscle, Isokinetic rehabilitation, Impedance control, Fuzzy sliding mode, Real-time control.

Manuscript received 16th July 2019, revised 30th October 2019 and 20th March 2020, accepted 15th June 2020.

* Corresponding author.

1. Introduction

Robots have been used extensively in various fields of research and industrial processes, and rehabilitation applications are no exception. The primary application of robots in rehabilitation is to minimize or eliminate direct human interactions and to reduce the overall cost of operations. Compared to traditional methods, the application of robots for rehabilitation purposes can improve the accuracy of exercises at a reasonable cost. Moreover, robots can efficiently monitor the quality of the expected tasks, which helps physicians to track a patient's recovery progress. In addition, robots can perform complex rehabilitation exercises iteratively. The precision and accuracy of the rehabilitation exercises play a significant role in the safety and the recovery progress of patients. Hence, such rehabilitation robots, to be reliable, must have a robust control system with a high level of accuracy for adjustment of the actuator's position and applied force. The first successful and commercialized robot-assisted physiotherapy device for arm recovery exercises, known as MIT-MANUS, was developed at the Massachusetts Institute of Technology (MIT) by Hogan *et al.* [1]. Since the invention of the robot in 1995, several researchers at MIT have modified the early design [2]. Saglia *et al.* designed a robot for ankle recovery exercises using a mechanism with redundant actuators [3]. In their design, electrical actuators were used, and it was suggested that springs should be added in connections between the platform and actuators to improve the compliance of the system. The application of the springs also reduced the bandwidth and decreased the controller's performance.

In most robotic applications, actuators get powered via an electrical motor, a hydraulic system, or a pneumatic system. In hydraulic actuators, as well as electrical actuators, designing the controller is straightforward, and the actuator can generate high loads. However, leakage is a common issue in the application of hydraulic systems. In addition, hydraulic and electrical systems intrinsically possess relatively high mass and impedance, which results in more operational complexities for physiotherapy and exoskeletons. On the other hand, pneumatic actuators are lighter and have lower inherent impedance. Complex controller design and the need for a high-pressure air supply unit are among the disadvantages of pneumatic systems. For stationary rehabilitation applications that are common in clinical spaces, the establishment of an air supply unit is achievable regardless of the size, and then the controller design remains the biggest challenge. As mentioned, electrical actuators are the most common tools used in rehabilitation devices. In series elastic actuators, an elastic element is added in series with an electrical actuator to reduce the impedance for ensuring the patient's safety during interaction with the robot. The main issue with this method is that the system's bandwidth—one of the advantages of electrical systems—is considerably reduced. To date, designs with incorporated pneumatic actuators are limited. Richardson *et al.* designed a 3-degree-of-freedom (DoF) rehabilitation robot for the top body. They used proportional derivative (PD) and impedance controllers [4]. Pneu-WREX was a 4-DoF pneumatic robot designed for upper limb rehabilitation exercises [5]. One of the most recent rehabilitation devices was designed by Norihiko Saga *et al.* In their design, a pneumatic cylinder was used to increase the safety and flexibility of the actuator and to reduce the device mass [6]. Henderson and Yueda designed and manufactured a rehabilitation robot in which an active force control algorithm was implemented to simulate isokinetic exercises using a pneumatic jack [7].

Pneumatic artificial muscles are pneumatic actuators that have been implemented in applications including exoskeleton robots and physiotherapy exercises. Advances in the application of elastic materials and understanding of their properties in the 1930s and 1940s led to the early introduction of pneumatic artificial muscles. In 1958, Richard Gaylord patented a pneumatic artificial muscle. In the early 1960s, Joseph Mckibben developed the application of pneumatic muscles and built a prototype [8]. The pneumatic muscles, due to their structure, possess lower weight



Figure 1. Pneumatic artificial muscle manufactured by Festo.

and provide the highest level of safety compared to other mechanisms. This is because of the reduced number of moving parts such as the electrical motor and hydraulic cylinder, which results in improved safety levels for rehabilitation purposes. Figure 1 shows a modern pneumatic muscle developed by Festo. An increase in pressure of the muscle's tube shortens the length of the muscle and generates tension force. A pneumatic artificial muscle (PAM) has a swellable membrane that is usually made of neoprene rubber surrounded by a nylon mesh. The inner section is completely closed on one side and the other side allows for gas (usually air) to flow in and out. When the compressed air enters the muscle from one side, the membrane swells. The mesh network on the membrane can be retracted and stretched. In addition, its threads are made of materials that can be considered strainless. Therefore, the threads do not feel any strain due to the pressure of the membrane, resulting in retracting or stretching of the mesh network. The set of these processes will eventually yield a back and forth motion during the change in the pressure of the PAM.

In the past 15 years, research has been conducted with the focus on the application of pneumatic muscles for lower body rehabilitation exercises [9]. Sawicki and Ferris designed an exoskeleton, called KAFO, for the rehabilitation of the ankle and knee [10]. Another example is the robot designed by Hussain and Xie for walking exercises [11]. In another research, Cao *et al.* designed an exoskeleton robot in which they proposed the proxy-based sliding mode control (PSMC) method for the control of the robot [12]. The PSMC method they proposed was a safe and model-free control strategy, which was used to ensure proper control of the exoskeleton. Zhao *et al.* designed a neck exerciser simulator using cable actuators and pneumatic muscles. In their design, the pneumatic muscle was used as a support, and it acted as spinal muscles [13].

Isokinetic exercise is a type of physiotherapy exercise and is referred to as the dynamic contraction of muscles at a fixed velocity. This kind of exercise, due to the exertion of the highest magnitudes of force to the injured limb within a wide range of motion, is the most effective method for regaining the strength and stamina of muscles [14]. For such exercises, a device that can simultaneously control force and velocity is required. In common devices, force and speed are controlled using an isokinetic dynamometer. The dynamometer's torque varies according to the patient's reaction force in such a way that the movement speed remains constant. In addition to the issues mentioned about electrical actuators, these systems are very expensive. Several studies have been carried out for the designing and building of physiography robots with isokinetic motion capabilities. Moughamir *et al.* invented a knee physiotherapy device, called Multi-Iso, with operations similar to those of an isokinetic dynamometer. They used fuzzy control techniques for controlling the position and speed [15]. The stability of the fuzzy controller for ensuring that the applied force was within the limit of the patient's maximum strength was not validated. Kikuchi *et al.* designed a 1-DoF robot for isokinetic exercises of arms using a

magnetorheological brake [16]. In all the mentioned circumstances, an electrical actuator with low compliance and a simple control system was used. Thudor and Andrea Deaconescu designed and built an isokinetic continuous passive motion rehabilitation device using a pneumatic muscle actuator in which a four-bar linkage mechanism was utilized to generate fixed velocity motion. Their experiment showed sinusoidal-shaped fluctuations of the velocity and relatively low levels of accuracy [17]. The rehabilitation robot AKROD was able to provide active knee rehabilitation via a variable damper component at the knee joint. The adjustable damping was achieved using an electrorheological smart brake [18]. Kara Lin Hall *et al.* designed a system for controlling a pneumatic muscle for the isokinetic rehabilitation of muscles. They used a sliding mode controller to apply a resistive force to the motion of a servo motor, which simulates knee muscles [19]. In this research, to obtain the maximum reliability and safety of the injured organ in contact with the device, a position-based impedance controller was proposed for rehabilitation applications.

Nonlinear dynamics and complexity of controlling pneumatic muscles have been the main obstacles in the development of pneumatic actuators in robotics. These issues are rooted in the compressibility property of the working fluid, which is air in most cases. Moreover, nonlinear elasticity of the membrane and mechanical characteristics of the combination of mesh/membrane are additional problems associated with these systems [20]. The advantages of using pneumatic muscles in physiotherapy robots have led many research studies worldwide toward modeling and controlling pneumatic muscles. The modeling of the pneumatic muscle's behavior has been studied in detail in previous research [21–24]. In [25], a piecewise affine model linearized around an operating point was used to control the motion of the actuator. The mentioned control methods were not as effective as expected mainly because of the nonlinear characteristic of pneumatic systems. In more recent studies, an adaptive control method was implemented by McDonnell [26] and Caldwell [27]. Krichel *et al.* [28] and Shen [29] developed a control system based on a nonlinear model for a pneumatic muscle of the linear antagonist joint. In [30], the sliding mode method was used by Lili and Yang to control the angle of the rotational antagonist joint. Similarly, Aschemann and Schindele used the sliding mode to control the position of a high-speed linear axis driven by pneumatic artificial muscle [31].

A sliding mode and nonlinear disturbance observer was proposed by Xing *et al.* for use in a specially designed hand rehabilitation device [32]. The MIMO Sliding Mode Controller for Gait Exoskeleton Driven by Pneumatic Muscles was proposed by Cao *et al.* [33]. In [34], an adaptive fuzzy algorithm was suggested to control the position of the pneumatic muscle. Chan and Repperger designed a PD and proportional integral (PI) control system for controlling the position of a pneumatic muscle [35]. Jiang *et al.* designed and built a prototype of a rehabilitation robot with rotational motion controlled by a fuzzy-neural algorithm [36]. Integrated intelligent nonlinear controller and adaptive recurrent neural network (NN) methods were experimentally compared by Ba *et al.* for a PAM [37]. To control the vertical position of the pneumatic muscle, Andrikopoulos *et al.* used model predictive control in [38] and an optimal control system in [25]. An echo state Gaussian-process-based nonlinear model predictive control was designed for the PAM by Huang *et al.* [39].

In sensitive applications such as rehabilitation, which demand high levels of reliability, control on the applied force from the robot is vital. The consideration of individual control parameters is very common and has been extensively studied in previous research. However, the position or force-based impedance control is very novel and has not been addressed in the literature for PAM. The need for high-fidelity control algorithms that are accurate within wide ranges of operating conditions is increasing, and this research aims to provide a controller specifically designed for rehabilitation applications. In the proposed controller design method, the impedance of the mechanism is considered for the control of the force and position of an artificial muscle.

Using the impedance control for rehabilitation devices at clinics enables the operator to provide different experiences to the patient by changing the impedance filter's characteristics artificially. In addition, this novel method enables enhanced control over the full range of the muscle's maximum displacement. This will result in a smaller length of muscle for a certain displacement range.

In this research, controlling a pneumatic muscle to be used for isokinetic rehabilitation exercises utilizing a fuzzy sliding mode was investigated. While designing the control system, the magnitude of the applied force from the actuator is also of importance. In this regard, the method of position-based impedance control was used to monitor the actuator's force during the reciprocating motion at a fixed velocity. Another important outcome of this research is considering the full displacement of the pneumatic muscle's motion while under control, which is equivalent to 25% of the muscle's initial length. The importance of the latter is that the dimensions of the muscle and consequently the overall size of the robot will be decreased if the length of the controlled motion is maximized.

In the following sections, first, the model used for the described control system and the experimental setup are explained. Then designing the fuzzy sliding mode controller based on the introduced model is discussed. Then, the position-based impedance control method is considered, and its algorithm is integrated with the position control algorithm. Finally, the experimental result of the designed control system is presented and discussed in detail.

2. Model of PAM

Figure 2 shows the schematic of the system under study before and after the displacement. The local zoomed view shows the angle of the muscle's thread. In this simplified model, a mass is vertically attached to a pneumatic muscle with the initial length L_0 . The most proper method for modeling the motion dynamics of a load vertically connected to a PAM was proposed by Chou and Hannaford in 1994 [21]. They derived a mathematical model between the force and displacement of the load based on the static equations of the PAM force.

$$F = \frac{\pi d_{90}^2 P}{4} (3 \cos^2 \theta - 1), \quad (1)$$

where F , P , and θ are the force, pressure, and angle of the muscle threads, respectively, and d_{90} is the minimum muscle diameter. Considering the effect of muscle membrane thickness, Chou and Hannaford proposed an enhanced version of (1) as follows,

$$F = \frac{\pi d_{90}^2 P}{4} (3 \cos^2 \theta - 1) + \pi P \left[d_{90} t_k \left(2 \sin \theta - \frac{1}{\sin \theta} \right) - t_k^2 \right], \quad (2)$$

where t_k is the PAM's thickness. However, this function is highly nonlinear, and its application for a model-based method result is complex. Therefore, a trade-off between control difficulty and tracking precision is required.

Shen [29] proposed a single input single output model for the PAM in the linear antagonistic joint by using the Chou–Hannaford algorithm. The control signal of the valve and the third derivative of the position are considered as the input and the output of the model, respectively. Incorporating the pressure dynamics and orifice equations into the proposed model makes it more suitable for experimental tests. As can be seen in (1), the force is a function of the muscle thread angle. However, he modified this equation to govern a function of the force versus the position of the muscle end as follows,

$$F = \left[\frac{3(L_0 - x)^2 - b^2}{4\pi n^2} \right] \cdot (P - P_{\text{atm}}), \quad (3)$$

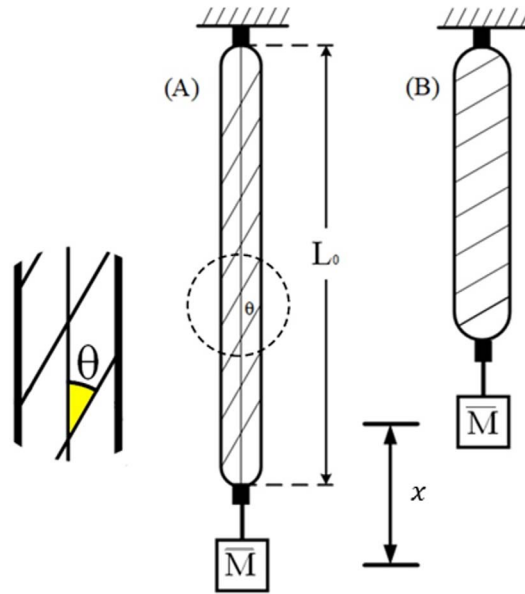


Figure 2. Schematic structure of the experimental setup: (A) muscle with initial length; (B) pressurized muscle.

where x , L_0 , b , n , and P_{atm} are the position, muscle length, thread length, number of threads, and environmental air pressure, respectively. In previous studies, this equation is used to calculate the force from the pressure sensor’s measurements. For instance, in [25], the same method was applied and results were reported.

In this paper, the vertical position of a mass connected to the PAM is studied. The system model has been extended based on the Chou–Hannaford equation and Shen’s method [29]. The dynamic equation of the system is given by

$$\ddot{x} = \frac{A}{M} \dot{m} - \frac{B}{M} \dot{x}, \tag{4}$$

where \bar{M} is the mass of the load and A and B can be described as in (5) and (6):

$$A = \frac{\gamma RT [3(L_0 - x)^2 - b^2]}{(L_0 - x) [b^2 - (L_0 - x)^2]}, \tag{5}$$

$$B = \frac{3[(L_0 - x)(P - P_{atm})]}{2\pi n^2} + \frac{\gamma [3(L_0 - x)^2 - b^2]^2 P}{4\pi n^2 (L_0 - x) [b^2 - (L_0 - x)^2]}. \tag{6}$$

In the above equations, T , R , and γ are the air temperature, the universal constant of gas, and the specific heat ratio coefficient, respectively. Furthermore, \dot{m} is the flow rate, which can be obtained from the following orifice equations of the valve.

$$\psi(P_u \cdot P_d) = \begin{cases} \sqrt{\frac{\gamma}{RT} \left(\frac{2}{\gamma+1}\right)^{\frac{\gamma+1}{\gamma-1}} C_f P_u} & \text{if } \frac{P_d}{P_u} \leq C_r \\ \sqrt{\frac{2\gamma}{RT(\gamma-1)}} \sqrt{1 - \left(\frac{P_d}{P_u}\right)^{\frac{\gamma-1}{\gamma}}} \left(\frac{P_d}{P_u}\right)^{\frac{1}{\gamma}} C_f P_u & \text{else.} \end{cases} \tag{7}$$

Here P_u , P_d , and C_f are the upstream pressure, the downstream pressure, and the discharge coefficient of the valve, respectively. C_r is the pressure ratio that identifies the unchoked versus choked flow regimes. In (7), for calculating ψ when the air is flowing into the muscle, we have

Table 1. Actual system parameters

Parameters	Value	Description
\bar{M}	5.1 kg	Mass of the load
P_s	6 bar	Supply pressure
n	1.06	Number of threads
γ	1.4	Specific heat coefficient
R	0.287 kJ/kg·K	Universal constant of gas
T	295 K	Air temperature
P_{atm}	1.01 bar	Environmental air pressure
C_f	0.294	Discharge coefficient of the valve
C_r	0.528	Pressure ratio
L_0	0.4 m	Muscle length
b	0.483 m	Thread length
A_v	[0–6.28] mm ²	Open area of the valve port

$P_u = P_s$ and $P_d = P$. Besides, when the air is flowing out, $P_u = P$ and $P_d = P_{\text{atm}}$ hold. Thus, this results in

$$\psi = \begin{cases} \psi(P_s, P) & \text{if } A_v \geq 0 \\ \psi(P, P_{\text{atm}}) & \text{if } A_v < 0 \end{cases} \quad (8)$$

$$\dot{m} = A_v \psi, \quad (9)$$

where A_v is equal to the open area of the valve port and P_s is the supply pressure. The atmospheric air pressure is considered fixed in all cases and is equal to the standard atmospheric air pressure as indicated in Table 1. The model parameters for the pneumatic muscle produced by Festo with 400 mm initial length used for numerical applications are listed in Table 1.

According to (4)–(8) and the relation of the input air mass flow, the dynamic system equation is written as

$$\ddot{x} = f(x) + g(x)\dot{m}, \quad (10)$$

where $x = [x \dot{x} \ddot{x} P]^T$ is the space state vector including load status, velocity, acceleration, and muscle pressure. $f(x)$ and $g(x)$ can be written as

$$\begin{aligned} f(x) &= -\frac{B}{M}\dot{x} \\ g(x) &= \frac{A}{M}. \end{aligned} \quad (11)$$

3. Experimental setup

A test bench with the following specifications was constructed to evaluate the performance of the proposed control method, as shown in Figure 3. The flow control valve made by Festo Company, MPYE-1/8 type, was used to control the inlet flow to the muscle. The maximum value of A_v , which indicates the opening area of the valve, was 6.28 mm². The range of the valve command signal was between 0 and 10 V, which closed at 5 V. This valve had two ports, and the input pressure to the PAM was provided through one of the ports. To eliminate the dead band at about 5 V, a compensator function was used as a supplementary. In order to measure the changes in muscle length due to the air pressure, Opkon's potentiometer transducer was utilized with an accuracy of 0.01 mm. The sensor data and command signal were transferred to the PC through a data acquisition (DAQ) card. The WIKA ECO-1 pressure sensor, output 4–20 mA, was employed to

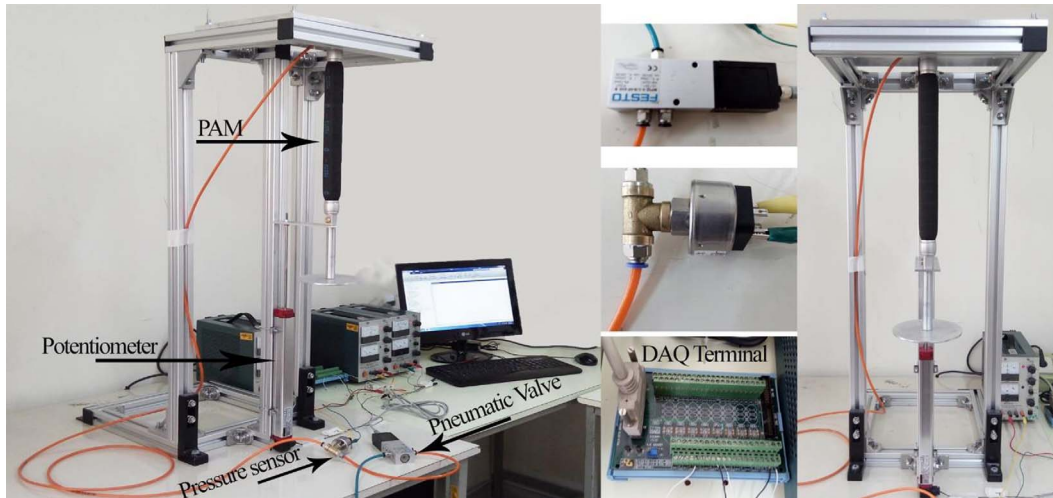


Figure 3. Experimental setup of the proposed structure.

Table 2. Experimental setup specification

Component	Manufacturer	Specification
PAM	Festo	DMSP40
Pneumatic valve	Festo	MPYE-5-1/8-HF-010-B
Potentiometer	Opkon	RTL 250D, 0.01 mm repeatability
DAQ card	Advantech	PCLD-8710
Pressure transducer	WIKA	ECO-1, 0–10 bar, 4–20 mA

measure the inlet air pressure to the PAM. To convert the output current of this sensor to voltage, a $250\ \Omega$ resistance should be inserted into the terminal of the DAQ card. The PAM manufactured by Festo Company with DMSP40 part number and 400 mm length was chosen for modeling purposes. The maximum course length of this muscle is 25% of its initial length and is equal to 100 mm. This paper aimed to develop a model that covers the muscle position throughout its course. The components of the experimental setup are listed in Table 2. It should be noted that the length of the pressurized air housing and related frictional losses and hence the location of the sensor on the housing did not have a noticeable impact on the sensor's reading. On the other hand, the length of the connecting wires from the sensor to the DAQ card caused increased noises and inversely affected the sensor's accuracy. So, in our test setup, we tried to put the sensor as close as possible to the electronic devices to reduce the wire length.

3.1. Valve's dead-band elimination

The pneumatic valve's dead band is one of the main issues in the lab experiments. Generally, proportional valves operate in a range of input voltage between 0 and 10 V. Changing the input voltage range to 0–5 V changes the valve output, respectively, between zero and the maximum value in one port, while voltage variation between 5 and 10 V changes the valve output between zero and the maximum value, respectively, in the other port. An input voltage of 5 V shuts the valve, and the output of the two ports becomes zero. These relations are valid for an ideal linear valve. However, in practice, the zero position of the valve (closed valve) does not occur at

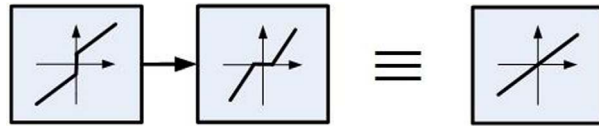


Figure 4. Dead-band compensation of proportional valves.

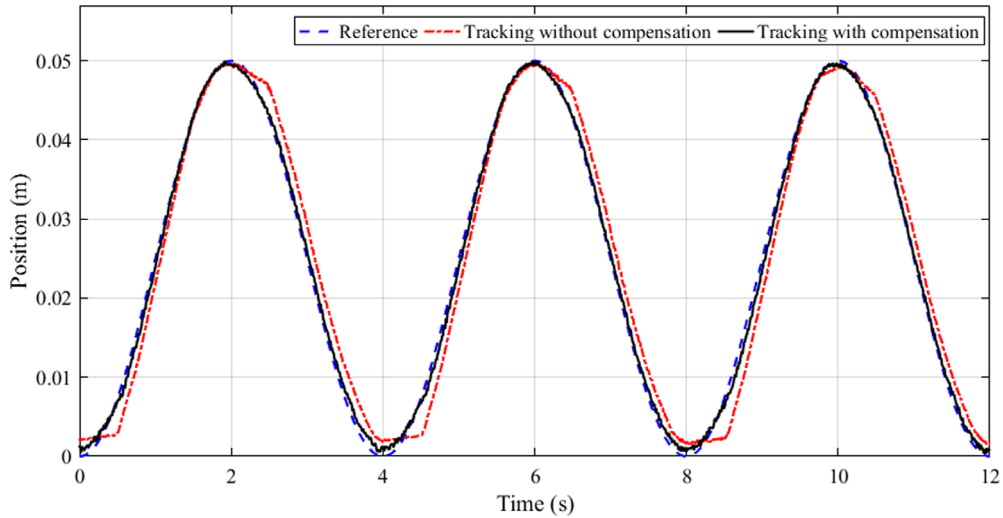


Figure 5. Effect of the dead-band compensator on the performance of the controller in the tracking of a sinusoidal reference signal.

Table 3. Neutral position and dead-band range of the servo valves

Joint	Dead band	Zero
1	0.2	5.37
2	0.24	5.25
3	0.36	5.44
4	0.34	5.13

exactly 5 V. According to the experiments, there is a voltage band near 5 V in which the valve remains closed. This nonlinear behavior reduces the controller’s performance. To reduce the negative effects of the zero band, different valves were tested to identify the dead band, and the results are presented in Table 3. Then, as shown in Figure 4, the nonlinear effects were compensated using a reverse function at the output of the controller.

To consider the effectiveness of the dead-zone compensator, a test was conducted using the test setup of a servo system. In the test, the ability to track a reference sinusoidal signal with and without using the compensator was investigated. The results of the test are shown in Figure 5, which indicate the enhanced behavior of the controller in the presence of the compensator.

4. Impedance control

Most of the rehabilitation robots are in direct contact with the injured limbs. This shows the importance of the safety and stability of the operations of rehabilitation robots compared to

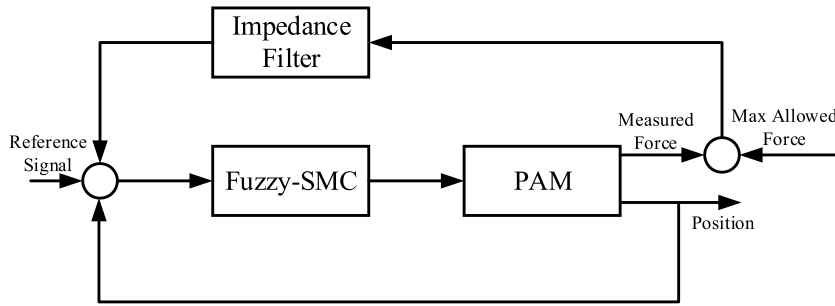


Figure 6. Position-based control block diagram [4].

other applications. Therefore, other than controlling and monitoring the position, the control system must be able to adjust the maximum applied force to the injured limbs. In the current application, the force and position are required to be simultaneously controlled. Because the force and position values at each time are mutually dependent, achieving the exact expected values of the force and position is impossible. Instead, the control system should compromise between the position and force reference signals [40].

There are three main methods for controlling the force and position at the same time: parallel, hybrid, and impedance control. In parallel control, the position signal is sacrificed for adjusting the force [41]. In hybrid control systems, both the force and position can be controlled in vertical orientations [42]. Impedance control does not control force or the position separately, but the dynamic relationship between these two is controlled [43]. In impedance control algorithms, a mass–spring–damper relation is defined between the force and position. In [40], Richardson investigated two types of impedance control based on position and force. It was found that the position-based impedance control performed better than force-based systems. Figure 6 shows the block diagram of an impedance control system.

The relation of force and position in a pneumatic muscle is defined by the transfer function as in (12),

$$\frac{x}{F_{\text{ext}}} = \frac{1}{Ms^2 + Cs + K}, \quad (12)$$

where x is the displacement as a result of external force F_{ext} . M , C , and K are mass, damping, and stiffness coefficients of the system, respectively. If the position is the system's input, Equation (12) can be rewritten as

$$\frac{F_{\text{ext}}}{x} = Ms^2 + Cs + K. \quad (13)$$

The position-based impedance control, if used in a no-contact condition (in the absence of an external force), operates similarly to a position controller. However, if subjected to loading, the value is defined as the maximum applied force from the actuator. A load sensor measures the magnitude of the applied force to the environment, and the deviation of the measured force from the reference maximum value is used for the configuration of the impedance filter. The impedance filter then transforms the force signal error into the position and changes the reference signal. In position-based impedance controllers, a compromise is made between the position signal and the maximum force to avoid exceeding the maximum allowable force. Thus, the controller's input is a signal different from the reference position signal. According to this, it is an essential requirement for an impedance controller to be able to track the position signal and limit the magnitude of the applied force in the absence of an impedance filter. Similarly, a force-based impedance control measures the position and modifies the reference force signals according to the position error.

As mentioned, previous studies showed that utilizing position-based impedance control systems has more advantages over force-based controllers for pneumatic systems [44]. Moreover, it was suggested to use a robust control algorithm for better handling of the changes in force. Here the parameters M , C , and K define the actuator's dynamic performance interacting with the patient's responses. Modifying these three parameters changes the patient's experience with the robot in terms of force, power, and velocity. "Impedance control fixes the relationship between the manipulator end-point and external forces as mass, spring, and damper system." [40].

In position-based impedance control, in addition to controlling the position of the actuator, the force feedback needs to be continuously monitored. Then, it is required to measure the real-time force magnitudes. As explained in the experimental setup section, a pressure sensor was used in this work to convert the air pressure into force. The relation between the force generated by the pneumatic muscle and air pressure is known from an analytical equation, and hence the application of an additional load sensor is not necessary. From (3), force can be calculated and can be applied to the impedance filter. From the application standpoint of this research, the final target parameters are the muscle's force, position, and velocity. The maximum designed force of the muscle corresponds to 3 bar air pressure. The maximum considered force—or the equivalent air pressure—was selected to ensure the safety of the patient or organ in contact with the muscle.

5. Designing a fuzzy sliding mode controller

As mentioned in the previous section, using a robust control method improves the performance of pneumatic systems controlled via position-based impedance methods. The sliding mode control method is an example of a robust control that has an effective approach in response to the perturbations within nonlinear systems such as the current pneumatic muscle mechanism in this research. Generally, the control algorithm of sliding mode methods includes an equivalent control u_{eq} and a switch control u_s . The equivalent control keeps the system states on the sliding surface while the switch control helps the system states attain the sliding surface.

One of the main issues in the application of sliding mode control is the chattering phenomenon. Since in this research the method of impedance control has been used, the ability of tracking the reference signals is essential. Accordingly, the negative effects of chattering on the controller are worse. In order to eliminate/reduce these effects, a fuzzy sliding mode is implemented. By adopting the fuzzy rule and based on the attaining condition, the switch gain is calculated. The calculated switch gain then reduces the chattering phenomenon and the system's disturbance.

In a control system, using the sliding mode method depends on the order and selection of the error integration of the sliding surface. We have

$$s = \left(\frac{d}{dt} + \lambda \right)^3 \int_0^t e dt, \quad (14)$$

where s denotes the sliding surface, λ is the controller bandwidth, and e is the position error,

$$e = x - x_d. \quad (15)$$

Rewriting (15) and differentiating with respect to the sliding surface, we have

$$\dot{s} = \ddot{e} + 3\lambda\ddot{e} + 3\lambda^2\dot{e} + \lambda^3e = 0. \quad (16)$$

After substitution and simplification, the controller's input equation is as follows,

$$A_v = \frac{1}{g(\mathbf{x})} (x_d - f(\mathbf{x}) - 3\lambda\ddot{e} - 3\lambda^2\dot{e} - \lambda^3e - K_{SM}\text{sgn}(s)), \quad (17)$$

where $f(\mathbf{x})$ and $g(\mathbf{x})$ are defined in (11), x_d is the desired position, and K_{SM} denotes the switching control gain constant and can be selected as

$$K_{SM} = \max|E(t)| + \eta. \quad (18)$$

Here $E(t)$ is the disturbance within the system and $\eta > 0$. In conventional sliding mode control, K_{SM} is used to compensate for the uncertainties and disturbances. With the integration used, we have

$$\hat{K}_{SM} = G \int_0^t \Delta K_{SM} dt, \quad (19)$$

where ΔK_{SM} is calculated from fuzzy rules and G is a proportionality coefficient and is determined by experiments. Therefore, the controller is designed as

$$A_v = \frac{1}{g(\mathbf{x})} (x_d - f(\mathbf{x}) - 3\lambda\ddot{e} - 3\lambda^2\dot{e} - \lambda^3e - \hat{K}_{SM}\text{sgn}(s)). \quad (20)$$

5.1. Stability analysis

The Lyapunov function is defined as

$$V = \frac{1}{2} s^2. \quad (21)$$

The derivative of the above function can be written as follows.

$$\dot{V} = s\dot{s}, \quad (22)$$

where \dot{s} is achieved in (16), and by substitution, we have

$$\dot{V} = s(\ddot{e} + 3\lambda\ddot{e} + 3\lambda^2\dot{e} + \lambda^3e) = s(f(\mathbf{x}) + g(\mathbf{x})A_v - \ddot{x}_d - E(t) + 3\lambda\ddot{e} + 3\lambda^2\dot{e} + \lambda^3e). \quad (23)$$

After simplification, we have

$$\dot{V} = s(-\hat{K}_{SM}(t)\text{sgn}(s) - E(t)) = -\hat{K}_{SM}(t)|s| - E(t)s \leq -\eta|s|. \quad (24)$$

In the above equation, the uncertainty function $E(t)$ is compensated by the switch gain, which ensures the sliding mode's condition. The switch gain is used to emit chattering and if the uncertainty depends on time, the switch gain can be calculated.

5.2. Designing a fuzzy system

The sliding mode's existing condition is defined as

$$s\dot{s} < 0. \quad (25)$$

If the condition of (25) is fulfilled, then the system states are on the sliding surface. To make the system states achieve the sliding surface, the selection of the switch gain should eliminate the system uncertainties [45]. To ensure the sliding mode's existence condition, the fuzzy rules are as stated below:

If $s\dot{s} > 0$, then $\hat{K}_{SM}(t)$ should be increased.

If $s\dot{s} < 0$, then $\hat{K}_{SM}(t)$ should be decreased.

The relations between $s\dot{s}$ and ΔK_{SM} can be designed using the above rules. In the current fuzzy system, $s\dot{s}$ is the input and ΔK_{SM} is the output. The inputs and outputs can be defined by fuzzy sets, respectively, as follows:

$$s\dot{s} = \{\text{NB NM Z PM PB}\}$$

$$\Delta K_{SM} = \{\text{NB NM Z PM PB}\},$$

where NB is negative big, NM is negative medium, Z is zero, PM is a positive medium, and PB is positive big. The fuzzy rule is selected as follows:

If $s\dot{s}$ is PB, ΔK_{SM} is PB.

If $s\dot{s}$ is PM, ΔK_{SM} is PM.

If $s\dot{s}$ is Z, ΔK_{SM} is Z.

If $s\dot{s}$ is NM, ΔK_{SM} is NM.

If $s\dot{s}$ is NB, ΔK_{SM} is NB.

In the following section, the behavior of the designed controller using the position-based impedance control of a pneumatic muscle is investigated and the lab results are presented. Results were obtained from three tests with different impedance coefficients.

6. Results and discussion

In this section, the result of the position-based impedance control of a pneumatic muscle is presented and compared, considering sinusoidal, trapezoidal, and saw-shaped inputs. In this regard, the control command is applied to the pneumatic valve via a DAQ card. The final position of the PAM, which moves a mounted weight, is measured by a linear potentiometer and its value is fed back using the DAQ card.

A sinusoidal signal is used to assess the behavior of the controller for tracking a reciprocating signal with a mild changing rate. The trapezoidal signal simulates an isokinetic motion with short resting time intervals, and the saw-shaped signal is selected for the simulation of continuous isokinetic exercises.

As mentioned in the literature review, the full stroke length of the muscle has not been considered comprehensively in previous studies. One of the main outcomes of the proposed position-based impedance control algorithm is the additional ability to maximize the controlled stroke length of the pneumatic muscle while controlling the impedance. In this research, the maximum displacement of the pneumatic muscle actuator is 100 mm, and the impedance control method used considered 95 mm of it. The main goal of the designed control system is to reach the target force/position values in the considered range of displacement. The ability of the controller to consider such a large stroke length will result in reduced size of the physiotherapy device. Furthermore, the implemented impedance control strategy prevents increased exerted force from the robot to the target environment, that is, the patient. Figures 7–15 show the results of tracking the mentioned reference signals. In all cases, the impedance constants are equal to $M = 7.5$ kg, $K = 3800$ N/m, and $C = 30$ N·s/m. The designed controller shows the best performance in terms of error and control criteria with these experimentally selected values. The optimized values are obtained from a parametric study for mass, stiffness, and damping coefficients. The result of the parametric study is provided in the following section as well.

The lab tests of the controller's performance on tracking a sinusoidal signal are shown in Figure 7, and the variation of the pneumatic muscle air pressure is shown in Figure 8. In Figure 8, the horizontal line shows the maximum allowable pressure to be applied to the pneumatic muscle. Figure 9 shows the position error in tracking a sinusoidal reference signal.

As shown in Figure 7, the application of the impedance filter resulted in a slight deviation from the reference sinusoidal signal at locations near the start and end of the stroke. Figure 8 shows that the muscle's maximum air pressure was kept near the maximum defined value. Here, a trade-off was made between the position tracking error and the deviation from maximum air pressure. Without considering the effect of the impedance filter, the deviation from the reference signal at the bottom and top of the sinusoidal signal peaks, which is shown in Figures 7 and 9,

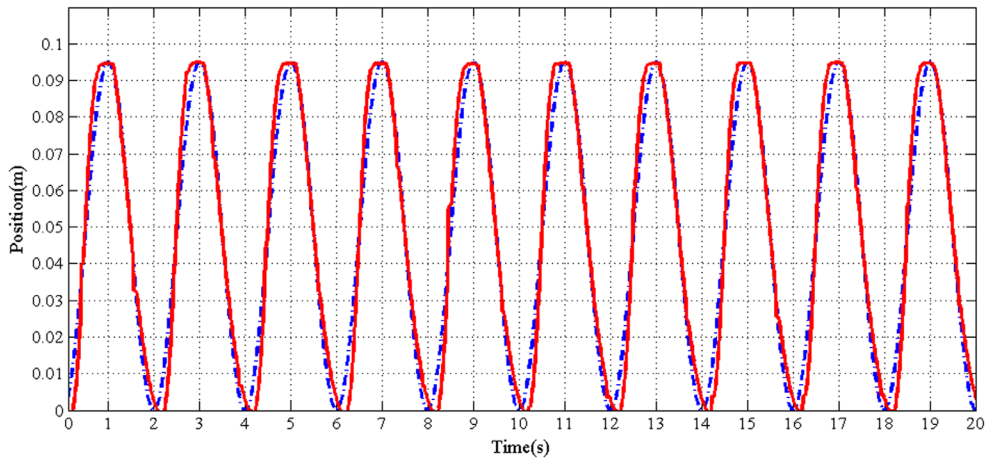


Figure 7. Controller's performance on the tracking of the sinusoidal reference signal.

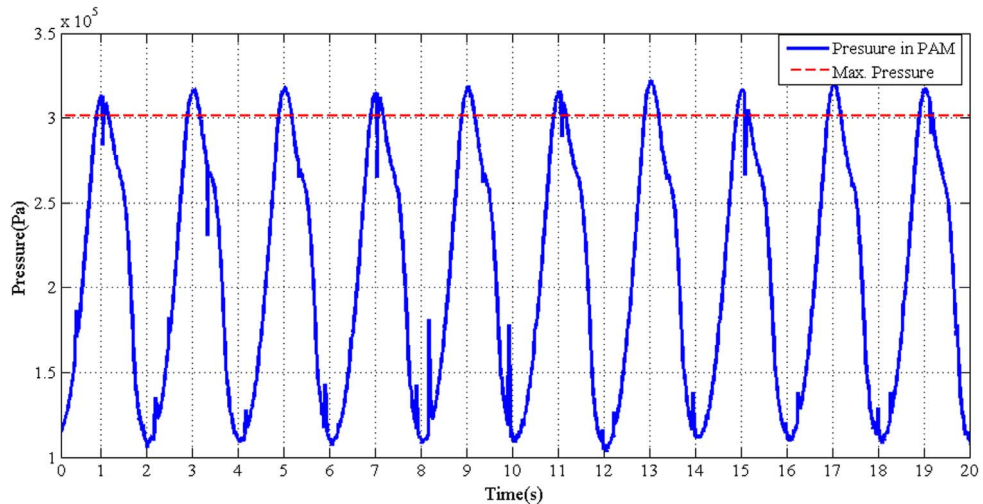


Figure 8. Muscle's air pressure variations during tracking of the sinusoidal reference signal.

could be due to different reasons. One reason could be the changing dynamics of the systems and the increasing uncertainties in the PAM model at the beginning and end of the range. Another reason may be hardware issues and inadequacies of laboratory equipment such as the presence of stiction in the pneumatic valve or clearance in the connection between the pneumatic muscle and the linear potentiometer. Similarly, in [46], it was reported that the behavior of the muscle was to some extent different from cycle to cycle due to variation in the hysteresis of the mechanical system. In addition to hardware issues, another reason is the intrinsic response of the position-based impedance controllers in which to avoid exceeded applied force, the error in the calculated force is converted to the position after passing the impedance filter. This will result in newly generated position commands, which are sent to the system. By examining how the controller performs in tracking the saw-shaped and trapezoidal signals, a better understanding of the issues can be gained. This behavior was observed during the other two reference signals, which simulate the isokinetic exercises. Figure 10 shows the result of the position tracking of the saw-shaped signal, and Figure 11 shows the associated pressure

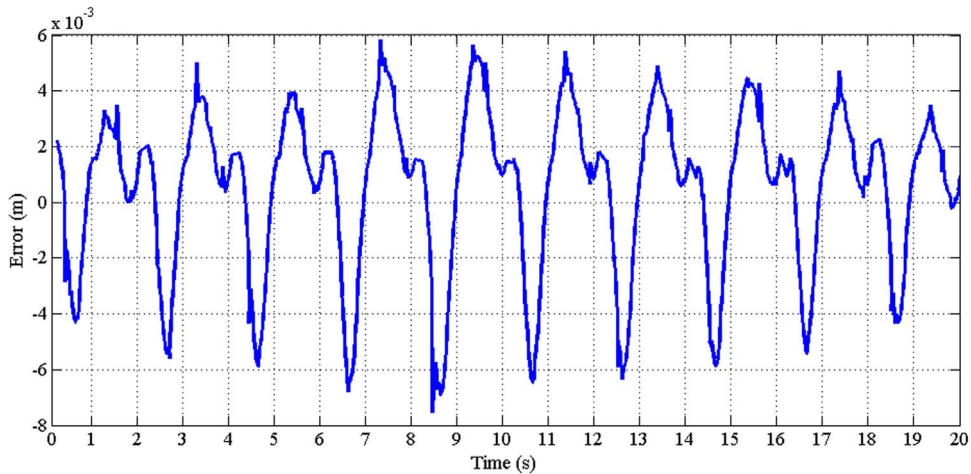


Figure 9. Position error in tracking a sinusoidal reference signal.

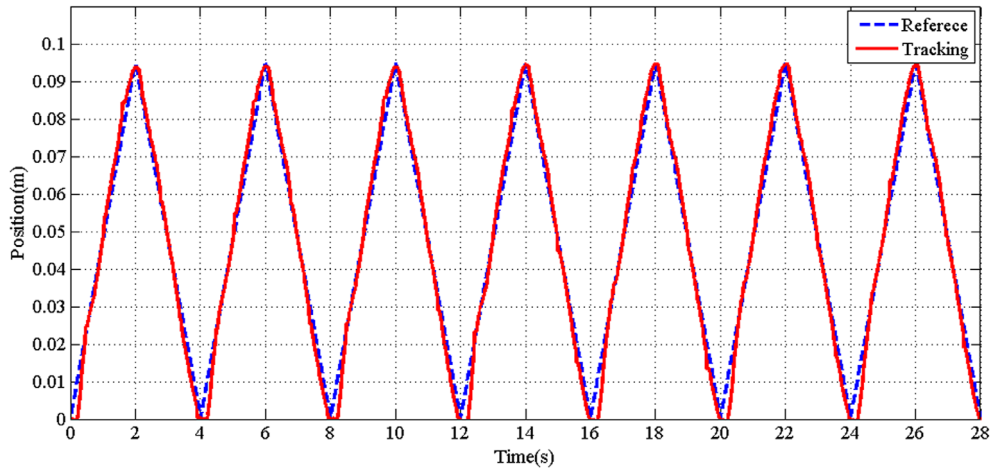


Figure 10. Controller's performance on the tracking of the saw-shaped reference signal.

results. Figure 12 shows the position error in the tracking of a saw-shaped reference signal. This signal represents a continuously reciprocating isokinetic motion.

As can be seen in Figure 10, the tracking of the position at the ends of the stroke was improved using the saw-shaped reference signal compared to the sinusoidal signals in terms of deviation from the reference signal. In Figure 12, the instantaneous error was higher at two points compared to that in Figure 9. However, in the calculations of the error, the average of the absolute error at the course's endpoints was considered. The mentioned error corresponding to Figure 9 was 0.0258 while it was calculated as 0.0113 for the results shown in Figure 12. However, the issue of increased air pressure more than the maximum value (increased force) at the stroke ends was increased (see Figure 11). The increased error of the force near the stroke ends was due to the stay time of the actuator at the transient point in which the displacement direction changes. The reason for the lower deviation in position tracking of the saw-shaped signal was that the actuator passed these points faster compared to the sinusoidal signal, and hence the impedance filter showed lower deviations and force error. The deviation at the initial locations of the stroke

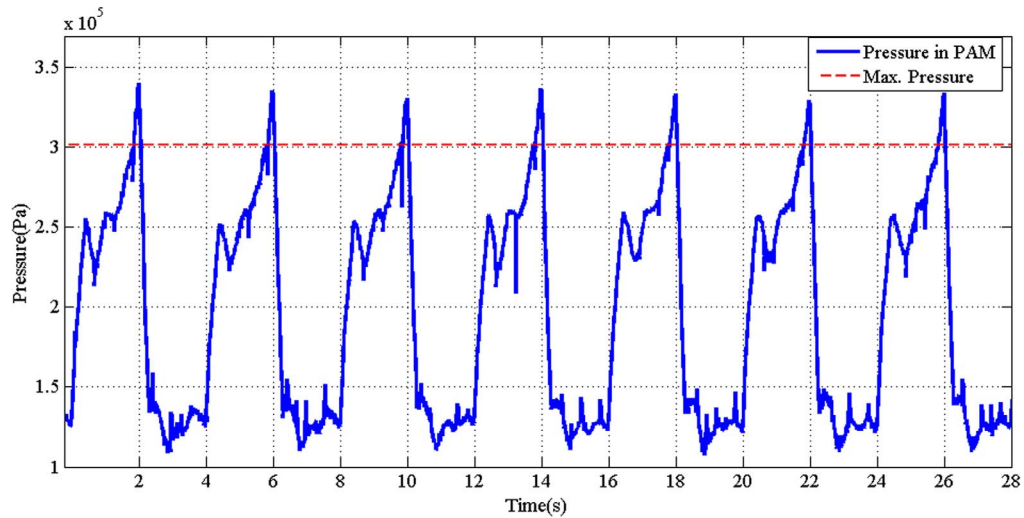


Figure 11. Muscle's air pressure variations during tracking of the saw-shaped reference signal.

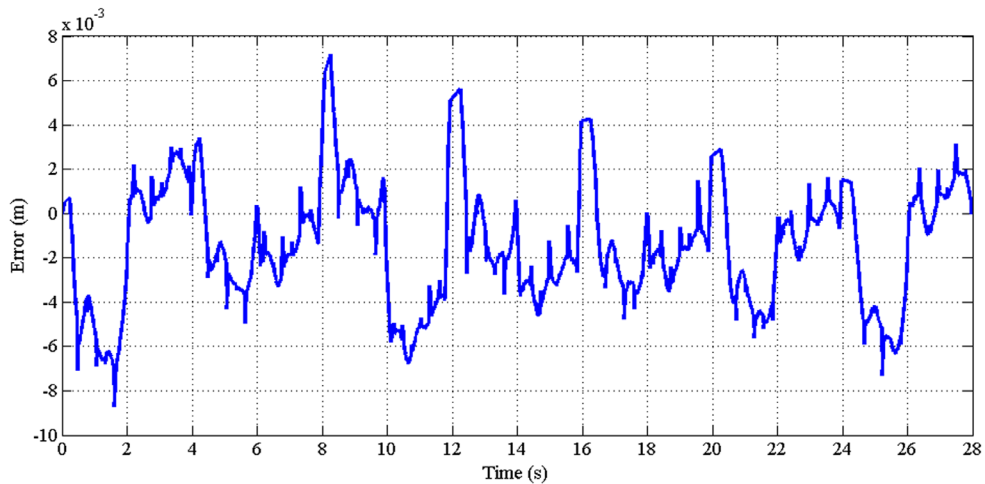


Figure 12. Position error in tracking a saw-shaped reference signal.

was higher than the end locations. The reason could be the dead band at the end position of the pneumatic valve. To reduce the effects of the dead band, a compensator was considered. However, experiments showed that its negative effects were not eliminated completely. Looking at the controller's behavior on the tracking of the trapezoidal position signal, effects of the valve's dead band on the deviation of pressure from the expected value at the ends of the stroke length, specifically the starting point, can be seen. Figures 13 and 14 represent a reciprocating constant speed motion (isokinetic) with stop intervals and pressure change while tracking the signal and its error, respectively. Figure 15 shows the position error in the tracking of a trapezoidal reference signal.

As expected, according to Figure 13, the deviation from the reference signal was higher at the beginning of the stroke. Figure 14 shows that the pressure magnitude exceeded the maximum defined pressure during a few short periods. It should be noted that from the lab tests, it was

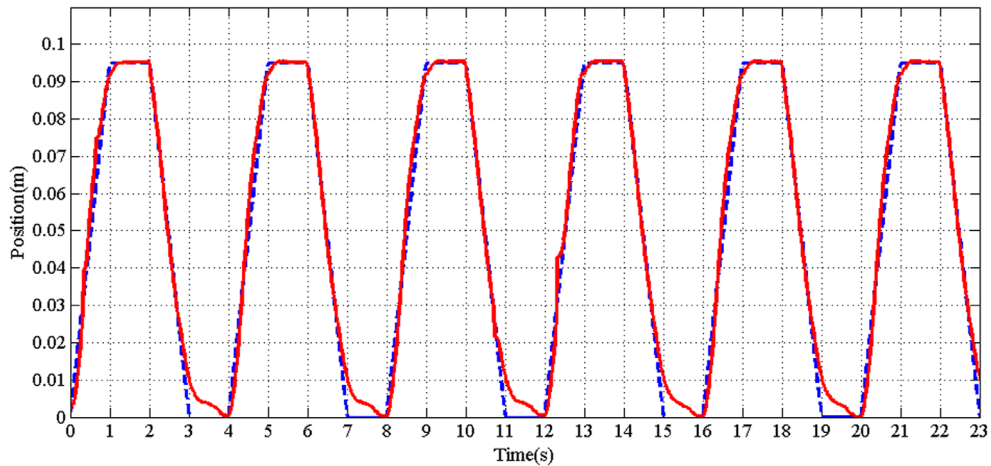


Figure 13. Controller's performance on the tracking of the trapezoidal reference signal.

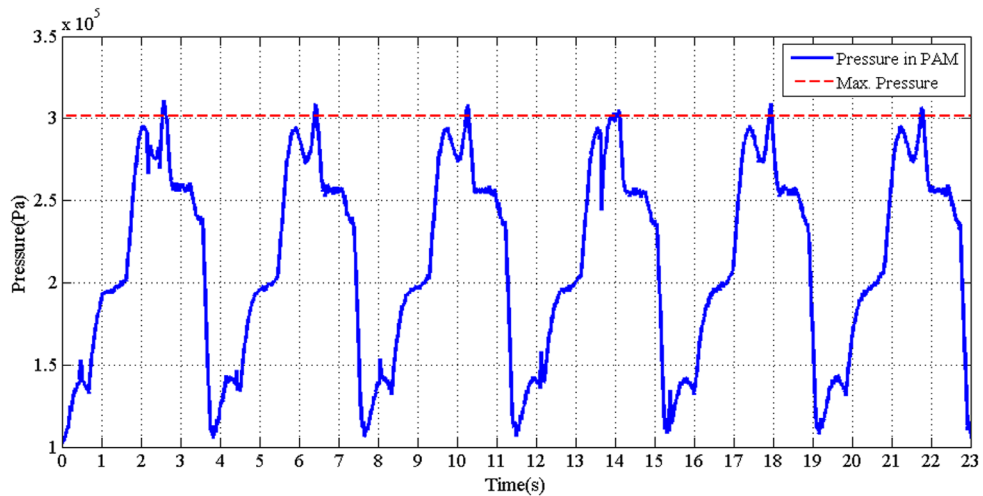


Figure 14. Muscle's air pressure variations during tracking of the trapezoidal reference signal.

discovered that the settling time is a major issue in controlling the muscle's position. Using the step reference signal with a value close to the maximum stroke length of the muscle, it was observed that the settling time was longer. To solve this issue, the controller needed to be adjusted. This tuning led to a decrease in the settling time in trapezoidal signal tracking as shown in Figure 13. In Figure 16, the performances of the proposed controller in this research and a common sliding mode controller were compared for tracking a step signal with the final position command of 95 mm.

It was explained in the controller design section that in the control system, the designer could modify the fuzzy rules and its membership functions' domain. Modifying the fuzzy control variables allowed the settling time to be minimized. In general, the higher deviation from the reference signals, specifically at the start of the displacements as shown in Figure 13, could be due to three reasons: the impedance filter deviation from the reference signal, the dead band of the pneumatic valve, and the settling time in system dynamics. The objective of this research

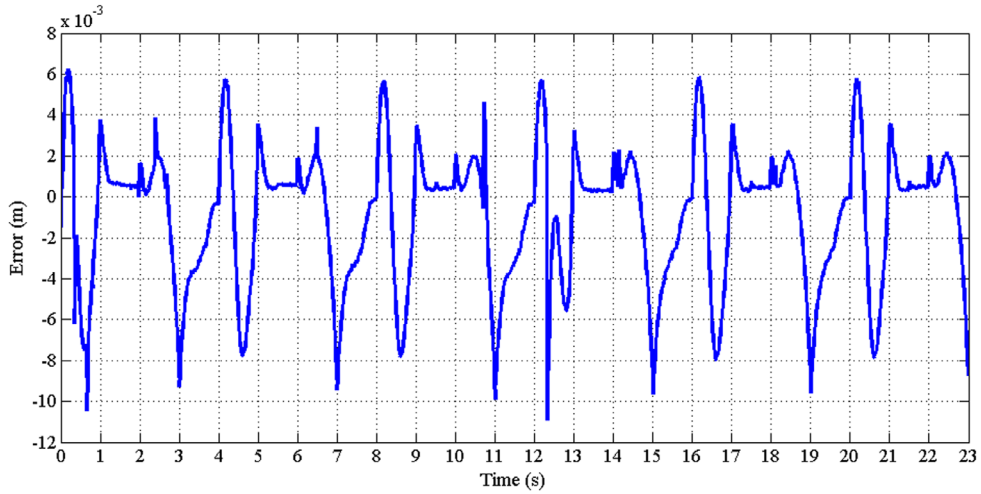


Figure 15. Position error in tracking a trapezoidal reference signal.

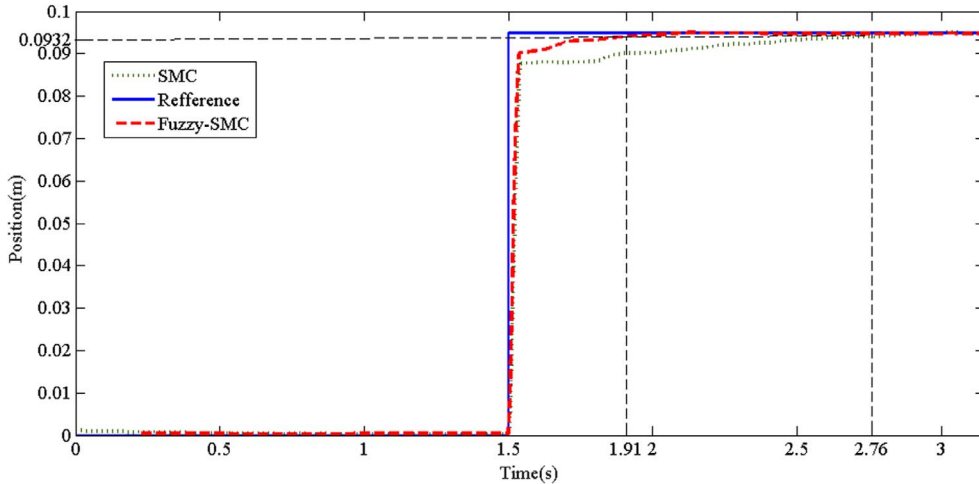


Figure 16. Comparison of the presented controller and a sliding mode controller on the tracking of a step reference signal (settling time for fuzzy-SMC is equal to 0.41 s and for SMC is equal to 1.26 s).

was to move the patient's injured limb at fixed velocity by performing isokinetic rehabilitation exercises, and according to Figures 10 and 13, the expected results were obtained with a desirable precision under two modes: with and without settling time at a constant velocity. The highest achieved accuracy in tracking the reference signals was calculated by 7.5% of error for the saw-shaped signal and 8.3% for the trapezoidal signal.

6.1. Impedance parameters

In this section, the effects of other impedance parameters including mass, stiffness, and damping are considered. A parametric study was conducted using a range of the three parameters as indicated in Table 4. The integral of time absolute error (ITAE) and the integral of absolute error

Table 4. Impedance parameters

C (N·s/m)	$M = 4.5$ kg, $K = 3800$ N/m		
	ITAE	IASE	Maximum error (%)
2	1.16	0.9074	15
10	0.9837	0.6604	8.5
20	0.508	0.412	6.2
30	0.223	0.103	4
M (kg)	$C = 30$ N·s/m, $K = 3000$ N/m		
	ITAE	IASE	Maximum error (%)
1.9	1.002	0.8214	13.5
5	0.885	0.6318	7.9
7.5	0.426	0.381	6.5
10	0.115	0.0927	5

(IASE) performance indexes are calculated for the parametric studies.

$$\text{ITAE} = \int |e(t) \cdot t| dt \quad (26)$$

$$\text{IASE} = \int |e(t)| dt.$$

According to Table 4, the controller outputs showed acceptable results by reducing the target damping up to within 1.9 kg of the controller. Further reduction caused persistent fluctuations around a position, and the controller was technically impractical. It should be mentioned that by changing the target stiffness and the damping, the target inertia can be changed as well. The zero damping of the system caused undesired fluctuations in the tracking of the signals and disturbed the system's operations.

Further investigation of the effects of impedance parameters on the performance of the controller was performed using an NN algorithm. Using such artificial intelligent methods facilitates the exploration of the design space utilizing various graphical tools such as 3D response surfaces and sensitivity charts [47]. The values provided in Table 4 were used as the initial design points to train the NN algorithm. The NN algorithm used M , C , and K values as inputs and the maximum error and IASE as the output criteria to interpolate between the design points. The total number of design points was increased to 1000 points. Figures 17 and 18 show the response surfaces and the sensitivity chart, respectively.

Figure 17(a)–(c) shows the influence of M , C , and K on the maximum error. For the surface graphs, only two of the input parameters are varied at a time while the other one remains constant at its mid-range based on Table 4 ($C = 15$ N·s/m, $M = 5.8$ kg, and $K = 3800$ N/m). The accuracy of the interpolations obtained from the NN increases by increasing the number of initial design points. Figure 17(a) shows that the error increases more linearly with stiffness at lower system damping. It is shown in Figures 17(b) and 17(c) that the reduction in the system's inertia results in a higher rate of error increase by variation of the damping and stiffness.

Figure 18 depicts the sensitivity of the outputs to the input parameters. The inner circle and the outer ring belong to the maximum error and the IASE as the outputs. Each of the colored segments belongs to one of the inputs, and the number on each of the segments shows the percentage of influence of that parameter. The larger the area means the higher the influence of the parameter. From the chart, stiffness had a nearly equal influence on both of the outputs. In addition, damping was identified as the most influential parameter, specifically on the IASE. The second important parameter in the system design was mass. The sensitivity chart provides useful

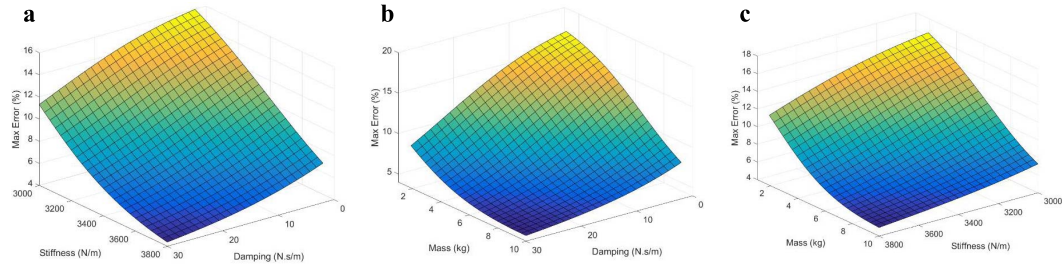


Figure 17. Effects of impedance parameters on maximum error. (a) Stiffness–damping ($M = 5.8$ kg), (b) mass–damping ($K = 3800$ N/m), (c) mass–stiffness ($C = 15$ N·s/m), versus the maximum error.

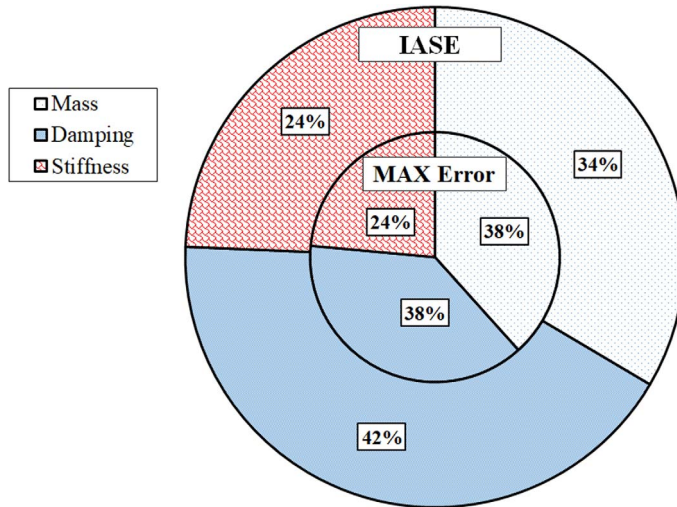


Figure 18. Sensitivity chart.

information that can be used for tuning the current system. At the given point (i.e., the mid-range point in Figure 18) of the parameters, the designer can decide to select a parameter that has the most influence on the outputs.

Overall, the performance of the controller was identified as satisfactory for tracking various reference signals under a wide range of impedance parameters, and the results were within an acceptable range with an estimated error of less than 10%. It should be noted that the maximum tracking error was less than 6% in many of the instances. This means that the proposed controller can be used for the control system of an isokinetic rehabilitation robot. Future work will use the proposed control algorithm in this paper and the implementation of it through the antagonistic joints for generating isokinetic rotational motion.

7. Conclusion

The position-based impedance control of a pneumatic artificial muscle using the fuzzy sliding mode controller was investigated. To analyze the performance of the controller, lab experiments measured vertical displacement of a mass attached to a pneumatic muscle controlled by the proposed controller. Due to the uncertainties and the simplifications during the modeling, the resistive fuzzy sliding mode control was implemented to enhance the accuracy of tracking

reference signals. The proposed method improved the chattering phenomena compared to the conventional sliding mode method, and the settling time was reduced by about 67%—from 1.26 s to 0.41 s—on the tracking of the step signal. Several position reference signals representing isokinetic rehabilitation exercises were tested. In addition, a parametric study was conducted to identify the effects of impedance parameters on the output criteria as well as the position error sensitivity to these parameters. Experiments showed that the designed controller was able to cover the full stroke length of the actuator with a maximum error of 8.5%. Moreover, a wide range of impedance parameters were used, and it was identified that the maximum error of velocity tracking was approximately 10%. During the experiments, the maximum applied force from the actuator was measured, and the value exceeded the maximum defined value a few times with a maximum value of 7%. In most instances of the tracking process, the maximum error was measured at 6%. Considering the requirements for rehabilitation in terms of the position tracking accuracy and force, the results of this research showed that the proposed controller can be used for designing an isokinetic rehabilitation robot with the impedance control algorithm.

Abbreviations

DAQ	data acquisition
DoF	degree of freedom
IASE	integral of absolute error
ITAE	integral of time absolute error
NN	neural network
PAM	pneumatic artificial muscle
PD	proportional derivative
PI	proportional integral

Symbols

F	Force
P	Pressure
θ	Angle of muscle threads
d_{90}	Minimum muscle diameter.
x	Position
L_0	Muscle length
b	Thread length
n	Number of threads
P_{atm}	Environmental air pressure
V	Muscle volume
\overline{M}	Mass of the load
M	Mass impedance parameter
C	Damping impedance parameter
K	Stiffness impedance parameter
g	Standard earth gravity
T	Air temperature
R	Universal constant of gas
γ	Specific heat coefficient
\dot{m}	Flow rate
A_v	Open area of valve port
F_{ext}	External force

References

- [1] H. Hogan, H. I. Kerbs, A. Sharon, J. Charnnarong, US Patent 5466213, November 1995.
- [2] J. Stein, H. I. Krebs, W. R. Frontera, S. E. Fasoli, R. Hughes, N. Hogan, "Comparison of two techniques of robot-aided upper limb exercise training after stroke", *Am. J. Phys. Med. Rehabil.* **83** (2004), no. 9, p. 720-728.
- [3] J. A. Saglia, N. G. Tsagarakis, J. S. Dai, D. G. Caldwell, "A high-performance redundantly actuated parallel mechanism for ankle rehabilitation", *Int. J. Robot. Res.* **28** (2009), no. 9, p. 1216-1227.
- [4] R. Richardson, M. Brown, B. Bhakta, M. Levesley, "Impedance control for a pneumatic robot-based around pole-placement joint space controllers", *Control Eng. Pract.* **13** (2005), p. 291-303.
- [5] E. T. Wolbrecht, D. J. Reinkensmeyer, J. E. Bobrow, "Pneumatic control of robots for rehabilitation", *Int. J. Robot. Res.* **29** (2010), no. 1, p. 23-38.
- [6] N. Saga, K. Kirihara, "Design of upper limb assistive device using a pneumatic cylinder", *J. Rehabil. Robot.* **1** (2013), no. 1, p. 9-18.
- [7] G. C. Henderson, J. Ueda, "Pneumatically powered robotic exercise device to induce a specific force profile in target lower extremity muscles", *Robotica* **32** (2014), no. 8, p. 1281-1299.
- [8] J. E. Takosoglu, P. A. Laski, S. Blasiak, G. Bracha, D. Pietrala, "Determining the static characteristics of pneumatic muscles", *Meas. Control* **49** (2016), no. 2, p. 62-71, Park YL.
- [9] B. R. Chen, D. Young, L. Stirling, R. J. Wood, E. Goldfield, R. Nagpal, "Bio-inspired active soft orthotic device for ankle foot pathologies", in *Intelligent Robots and Systems (IROS), 2011 IEEE/RSJ International Conference*, IEEE, 2011, p. 4488-4495.
- [10] G. S. Sawicki, D. P. Ferris, "A pneumatically powered knee-ankle-foot orthosis (KAFO) with myoelectric activation and inhibition", *J. Neuroeng. Rehabil.* **6** (2009), no. 1, article ID 23.
- [11] S. Hussain, S. Q. Xie, P. K. Jamwal, "Robust nonlinear control of an intrinsically compliant robotic gait training orthosis", *IEEE Trans. Syst. Man Cybern. Syst.* **43** (2013), no. 3, p. 655-665.
- [12] Y. Cao, J. Huang, Z. Huang, X. Tu, S. Mohammed, "Optimizing control of passive gait training exoskeleton driven by pneumatic muscles using switch-mode firefly algorithm", *Robotica* **37** (2009), no. 12, p. 2087-2103.
- [13] X. Zhao, B. Zi, L. Qian, "Design, analysis, and control of a cable-driven parallel platform with a pneumatic muscle active support", *Robotica* **35** (2017), no. 4, p. 744-765.
- [14] C. Xiong, X. Jiang, R. Sun, X. Huang, Y. Xiong, "Control methods for exoskeleton rehabilitation robot driven with pneumatic muscles", *Ind. Robot Int. J.* **36** (2009), no. 3, p. 210-220.
- [15] S. Moughamir, J. Zaytoon, N. Manamanni, L. Afilal, "A system approach for control development of lower-limbs training machines", *Control Eng. Pract.* **10** (2002), no. 3, p. 287-299.
- [16] T. Kikuchi, K. Oda, J. Furusho, "Leg-robot for demonstration of spastic movements of brain-injured patients with compact magnetorheological fluid clutch", *Adv. Robot.* **24** (2010), no. 5-6, p. 671-686.
- [17] T. Deaconescu, A. Deaconescu, "Pneumatic muscle actuated isokinetic equipment for the rehabilitation of patients with disabilities of the bearing joints", in *Proceedings of the International MultiConference of Engineers and Computer Scientists*, Lecture Notes in Engineering and Computer Science, vol. 2, The International Association of Engineers (IAENG), 2009, ISSN: 2078-0966.
- [18] J. Nikitczuk, B. Weinberg, P. K. Canavan, C. Mavroidis, "Active knee rehabilitation orthotic device with variable damping characteristics implemented via an electrorheological fluid", *IEEE/ASME Trans. Mechatronics* **15** (2010), no. 6, p. 952-960.
- [19] K. L. Hall, C. A. Phillips, D. B. Reynolds, S. R. Mohler, A. T. Neidhard-Doll, "Pneumatic muscle actuator (PMA) task-specific resistance for potential use in microgravity exercise", *Aviat. Space Environ. Med.* **83** (2012), no. 7, p. 696-701.
- [20] E. T. Wolbrecht, D. J. Reinkensmeyer, J. E. Bobrow, "Pneumatic control of robots for rehabilitation", *Int. J. Robot. Res.* **29** (2010), no. 1, p. 23-38.
- [21] C. P. Chou, B. Hannaford, "Static and dynamic characteristics of McKibben pneumatic artificial muscles", in *Proceedings of the 1994 IEEE International Conference on Robotics and Automation*, San Diego, CA, IEEE, 1994.
- [22] B. Tondu, P. Lopez, "The McKibben muscle and its use in actuating robot-arms showing similarities with human arm behavior", *Ind. Robot Int. J.* **24** (1997), no. 6, p. 432-439.
- [23] H. F. J. Schulte, "The characteristics of the McKibben artificial muscle", in *The Application of External Power in Prosthetics and Orthotics*, Nat. Acad. Sci.-Nat. Res. Council., Washington, DC, 1961.
- [24] A. Hosovsky, M. Havran, "Hill's muscle model-based modeling of pneumatic artificial muscle", *Ann. DAAAM Proc.* (2011), p. 1005-1007.
- [25] G. Andrikopoulos, G. Nikolakopoulos, I. Arvanitakis, S. Manesis, "Piecewise affine modeling and constrained optimal control for a pneumatic artificial muscle", *IEEE Trans. Ind. Electron.* **61** (2014), no. 2, p. 904-916.
- [26] B. W. McDonnell, J. E. Bobrow, "Adaptive tracking control of an air powered robot actuator", *Trans. ASME, J. Dyn. Syst. Meas. Control* **115** (1993), no. 3, p. 427-433.
- [27] D. G. Caldwell, G. A. Medrano-Cerda, M. Goodwin, "Control of pneumatic muscle actuators", *IEEE Control Syst.* **15** (1995), no. 1, p. 40-48.

- [28] S. V. Krichel, O. Sawodny, A. Hildebrandt, "Tracking control of a pneumatic muscle actuator using one servo valve", in *American Control Conference (ACC), 2010*, IEEE, 2010, p. 4385-4390.
- [29] X. Shen, "Nonlinear model-based control of pneumatic artificial muscle servo systems", *Control Eng. Pract.* **18** (2010), no. 3, p. 311-317.
- [30] J. H. Lilly, L. Yang, "Sliding mode tracking for pneumatic muscle actuators in opposing pair configuration", *IEEE Trans. Control Syst. Technol.* **13** (2005), no. 4, p. 550-558.
- [31] H. Aschemann, D. Schindele, "Sliding-mode control of a high-speed linear axis driven by pneumatic muscle actuators", *IEEE Trans. Ind. Electron.* **55** (2008), no. 11, p. 3855-3864.
- [32] K. Xing, J. Huang, Y. Wang, J. Wu, Q. Xu, J. He, "Tracking control of pneumatic artificial muscle actuators based on sliding mode and non-linear disturbance observer", *IET Control Theory Appl.* **4** (2010), no. 10, p. 2058-2070.
- [33] J. Cao, S. Q. Xie, R. Das, "MIMO sliding mode controller for gait exoskeleton driven by pneumatic muscles", *IEEE Trans. Control Syst. Technol.* **26** (2017), no. 1, p. 274-281.
- [34] K. Balasubramanian, K. S. Rattan, "Trajectory tracking control of a pneumatic muscle system using fuzzy logic", in *Fuzzy Information Processing Society, 2005. NAFIPS 2005. Annual Meeting of the North American*, IEEE, 2005, p. 472-477.
- [35] S. W. Chan, D. W. Repperger, "Fuzzy PD+I learning control for a pneumatic muscle", in *IEEE International Conference on Fuzzy Systems*, IEEE, 2003.
- [36] X. Jiang, Z. Wang, C. Zhang, L. Yang, "Fuzzy neural network control of the rehabilitation robotic arm driven by pneumatic muscles", *Ind. Robot Int. J.* **42** (2015), no. 1, p. 36-43.
- [37] D. X. Ba, T. Q. Dinh, K. K. Ahn, "An integrated intelligent nonlinear control method for a pneumatic artificial muscle", *IEEE/ASME Trans. Mechatronics* **21** (2016), no. 4, p. 1835-1845.
- [38] G. Andrikopoulos, G. Nikolakopoulos, S. Manesis, "Pneumatic artificial muscles: a switching model predictive control approach", *Control Eng. Pract.* **21** (2013), no. 12, p. 1653-1664.
- [39] J. Huang, Y. Cao, C. Xiong, H. T. Zhang, "An echo state Gaussian process-based nonlinear model predictive control for pneumatic muscle actuators", *IEEE Trans. Autom. Sci. Eng.* **16** (2018), no. 3, p. 1071-1084.
- [40] R. Richardson, "Actuation and control for robotic physiotherapy", Doctoral dissertation, University of Leeds, 2001.
- [41] S. Chiavervini, L. Sciavicco, "The parallel approach to force/position control of robotic manipulators", *IEEE Trans. Robot. Autom.* **9** (1993), no. 4, p. 361-373.
- [42] M. H. Raibert, J. J. Craig, "Hybrid position/force control of manipulators", *Trans. ASME, J. Dyn. Syst. Meas. Control* **103** (1981), p. 126-133.
- [43] N. Hogan, "Impedance control: an approach to manipulation: Part II—Implementation", *Trans. ASME, J. Dyn. Syst. Meas. Control* **107** (1985), no. 1, p. 8-16.
- [44] B. Heinrichs, N. Sepehri, A. B. Thornton-Trump, "Position-based impedance control of an industrial hydraulic manipulator", *IEEE Control Syst.* **17** (1997), no. 1, p. 46-52.
- [45] J. Liu, X. Wang, *Advanced Sliding Mode Control for Mechanical Systems: Design, Analysis and MATLAB Simulation*, Springer Science & Business Media, 2012.
- [46] G. Andrikopoulos, G. Nikolakopoulos, S. Manesis, "Novel considerations on static force modeling of pneumatic muscle actuators", *IEEE/ASME Trans. Mechatronics* **21** (2016), no. 6, p. 2647-2659.
- [47] N. Z. Meymian, N. N. Clark, T. Musho, M. Darzi, D. Johnson, P. Famouri, "An optimization method for flexural bearing design for high-stroke high-frequency applications", *Cryogenics* **95** (2018), p. 82-94.